WIDE FIELD IMAGING AND THE VELOCITY STRUCTURE IN THE COMA OF HALE–BOPP

WALTER M. HARRIS, JEFFREY P. MORGENTHALER, FRANK SCHERB and CHRISTOPHER ANDERSON
University of Wisconsin-Madison, 1150 University Ave. Madison, WI 53706, USA
E-mail: wharris@sal.wisc.edu

RONALD J. OLIVERSEN
Goddard Spaceflight Center, Code 681, Greenbelt, MD 20771, USA

(Received 18 March 2002; Accepted 3 July 2002)

Abstract. The comae of very active comets have a substantially more complex coma than their weaker cousins. The primary cause of this is photolytic heating and collisions that occur over an ever-larger volume of the coma as Q_{H_2O} increases. Collisions with the photochemical daughters of water in this region modify the radial distributions and outflow velocity of each species, excite and quench metastable emissions, and introduce velocity gradients from photolytic heating. Comet Hale–Bopp was the first comet for which the collisional coma was both spatially resolvable and comparable in extent to the scale lengths of major coma species. In the case of this object, the classical assumptions that make it possible to invert radial emission line profiles, brightnesses, and lineshapes to production rate and velocity either do not hold or require adjustment to work. Here we describe how a large collision zone modifies the coma, how it affects the classical methods for obtaining production rate and velocity, and discuss how wide field imaging may be combined with modified versions of simple models to address the complications and extract some structural information.

1. Introduction

Comet Hale–Bopp was among the most active comets ever observed, with a peak water production rate of $Q_{H_2O} = 10^{31}$ s^{-1} near perihelion (Colom et al., 1999; Combi et al., 2000; Dello Russo et al., 2000; Morgenthaler et al., 2001; Harris et al., 2002), that was several times greater than the highest production rate observed from 1P/Halley in 1986 (e.g., Craven and Frank, 1986; McFadden et al., 1986; Feldman et al., 1986). Such a high production rate has both positive and negative implications for determining the characteristics of the coma. In particular, high water production rates correlate with an increased ability to detect minor coma species, map detailed small-scale structures in the inner coma at high signal to noise, and to measure distributions of major species out to greater nuclear distances. On the other hand, high gas production was known before Hale–Bopp to correlate with increasing coma outflow velocities (Bockelée-Morvan et al., 1990), due presumably to photolytic heating over an increasingly extended, but not spatially resolved, region near the nucleus. Hale–Bopp represents an extreme case

Earth, Moon and Planets **90:** 45–56, 2002.

where the collisional region becomes large enough to be observed directly, and, more significantly, begins to approach the photochemical scale lengths of major coma species including, H_2O, OH, CO_2, and HCN. When this occurs, the velocity distribution of the coma ceases to be determinable with the standard assumptions of parent-daughter energy/velocity breakdown, vectorial flow, and a quasi iso-velocity ballistic coma that are used to invert distributions and aperture averaged line profiles directly to gas production and dynamics.

This paper discusses the background simplifying assumptions used to derive $Q_{\rm gas}$ for weaker comets and how the extreme nature of Hale–Bopp's coma affects them. We then examine how wide field data on active comets, which provide crucial information on the outer coma distribution and the velocity distribution of key species, can be modeled either with modified spherical expansion simulations or advanced codes that account for collisional effects.

2. Inversion Techniques and Assumptions

For the typical low activity comet, gas production rates and velocities can be determined reliably through a combination of spatial brightness mapping and simple models.

Production Rate. A species brightness distribution can be obtained using either variable-width aperture photometry (Morgenthaler et al., 2001; Schultz et al., 1993) or ring-sum extraction of the radial brightness away from the nucleus (e.g., Harris et al., 2002; Festou, 1981). If the emissions are prompt (metastable), then the column densities follow directly from the brightness (Schultz et al., 1993), while resonance line column densities are determined from the heliocentric velocity corrected fluorescence efficiencies (e.g., Schleicher and A'Hearn, 1988). These column densities are then inverted back to a species production rate using radial (Haser, 1957) or vectorialized (Festou, 1981) spherical expansion models that rely on known values of photochemical lifetime and parent-daughter branching ratios. Despite the simplicity of these models, they consistently produce results that compare favorably to those from more detailed simulations.

Outflow Velocity. The *average* velocity of a particular species can be directly measured with very high spectral resolution observations of the field-averaged emission line width (Bockelée-Morvan et al., 1990; Biver et al., 1999; Colom et al., 1999; Morgenthaler et al., 2001). Acceleration in the flow can be detected by comparing profiles obtained over fields of view with different radii. It is also possible to obtain the mean outflow velocity by fitting the radial brightness distribution with spherical expansion models. However, expansion models will provide unique results only when either the entire profile is measured, when the velocity parameter space is bounded by other measurements (Harris et al., 2002), or if the outflow velocity

is pegged to an outside measurement or relationship such as the $V = 0.87\ R_{\rm H}^{-0.5}$ (where $R_{\rm H}$ is heliocentric distance) formula of Budzien et al. (1994).

For the above techniques to provide unique, physically descriptive results that compare well with those of far more detailed photochemical simulations (Combi et al., 1993), several assumptions must hold. These include:

- The flow is completely ballistic.
- The velocity of each inner coma parent species is equal to the bulk water outflow.
- Daughter species velocity distributions are the convolution of the water velocity with the spherically symmetric vectorialized velocity that comes from excess energy of photodissociation.
- The mean velocity of a species is approximately uniform throughout the coma.
- Metastable emissions are neither quenched nor stimulated to a significant degree beyond the immediate vicinity of the nucleus.

3. The Role of Collisions

For most comets, there is a region known as the *collision sphere* near the nucleus, inside which collisions dominate and neutrals and ions of different energies are mixed together into a single thermalized flow. Provided that this is not spatially resolvable from the nucleus and is small compared with the photochemical scale lengths of the major coma species, no velocity gradients are introduced and the daughter species velocity distributions are not affected. In this unresolved case, the collision sphere acts only to increase the bulk coma outflow velocity along with $Q_{\rm H_2O}$ (Bockelée-Morvan et al., 1990; Cochran and Schleicher, 1993). However, as gas production increases, the size of the collision sphere does as well. This increase can be described by a simple relationship

$$R_C = \frac{\sigma Q_{\rm H_2O}}{4\pi V}, \tag{1}$$

where σ is the ballistic cross section and V is the outflow velocity (Whipple and Huebner, 1976). This equation is a simplification, because, while collisional mixing occurs throughout the sphere, it does not account for differences between the inner 10% of the sphere that is thermalized (Combi et al., 1999) and the outermost regions where the flow is nearly ballistic and collisions are an occasional occurrence.

For even highly active comets, such as P/Halley, the collision sphere is very small in extent compared with relevant distance scales in the coma. With the above equation, $R_C = 10^4$ km for the highest measured activity from Halley ($Q_{\rm H_2O} = 1.5 \times 10^{30}\ {\rm s}^{-1}$) (Feldman and Brune, 1976), a value confirmed with *in situ* measurements and models (Hodges, 1990). However, circumstances were very different for comet Hale–Bopp, where there is general agreement that $Q_{\rm H_2O}$ was $= 1.5 \times 10^{31}\ {\rm s}^{-1}$ at

perihelion (e.g., Harris et al., 2002) and the collision sphere radius was therefore $R_C = 10^5$ km. For the geocentric distance of Hale–Bopp at perihelion (1.4 AU), such a collision sphere would have an easily resolvable angular diameter of roughly 3 archmin.

4. Consequences for the Active Comet Coma

The implications of $R_C > 10^5$ km for the structure of a coma are significant. Such a collision sphere is large enough to be both spatially resolvable and comparable to the photochemical lifetimes of major species. This is particularly important for water, which has a lifetime of $\tau_{H_2O} = 8.6 \times 10^4$ s at solar minimum and 1 AU (Huebner et al., 1992), and is the most abundant coma constituent. Even allowing for significant acceleration to >1 km/s across this region, R_C is comparable to the water scale length ($S_{H_2O} = \tau_{H_2O} V_{H_2O}$), and thus much of it is dissociated in an at least partially collisional environment. Furthermore the OH lifetime is also short ($\tau_{OH} = 1.3 \times 10^5$ s (Huebner et al., 1992), and much of it is *also* dissociated in the collisional region. The end result is that H_2O ends up thermalized with the products of its own photochemistry, including OH, H, O, H_2, and H_2O^+.

These circumstances generally invalidate the necessary assumptions described above for the determination of Q and V, especially as they relate to water and its daughter products. The outflow cannot be approximated as ballistic, nor is it uniform with increasing radial distance. The amount of energy being re-thermalized from water daughter products increases across the sphere, resulting in a steady increase in coma outflow velocity with cometocentric distance (e.g., Combi et al., 1999). Because the daughters are thermalized back into the flow, it is also not valid to assume that their velocity distribution is either vectorialized or directly related to the excess energy of dissociation. Indeed, aperture averaged line profile measurements will contain elements of the vectorial and thermalized velocity distributions. Given that the thermalized velocity changes with distance, both the velocity line shape *and* the radial brightness distribution inside the aperture must be known to correctly interpret the data, particularly in the inner comawhere the gradients are largest (Biver et al., 1999).

Collisions have extreme consequences for metastable emissions as well. For very strongly quenched features, such as 18 cm line of OH (Schloerb, 1988; Schloerb et al., 1999), observations sample only the outer regions of coma, effectively biasing their measurement to regions beyond the collision zone and any acceleration. In the case of Hale–Bopp, the radio OH quenching radius was larger than 5 $\times 10^5$ km, which was well past the edge of the collision sphere. The use of other diagnostic prompt emissions such as OI (Morgenthaler et al., 2001; Schultz, et al., 1993) and CI (Oliversen et al., 2002), to determine their parent production rates is also complicated by collisional quenching and to some extent by both chemical

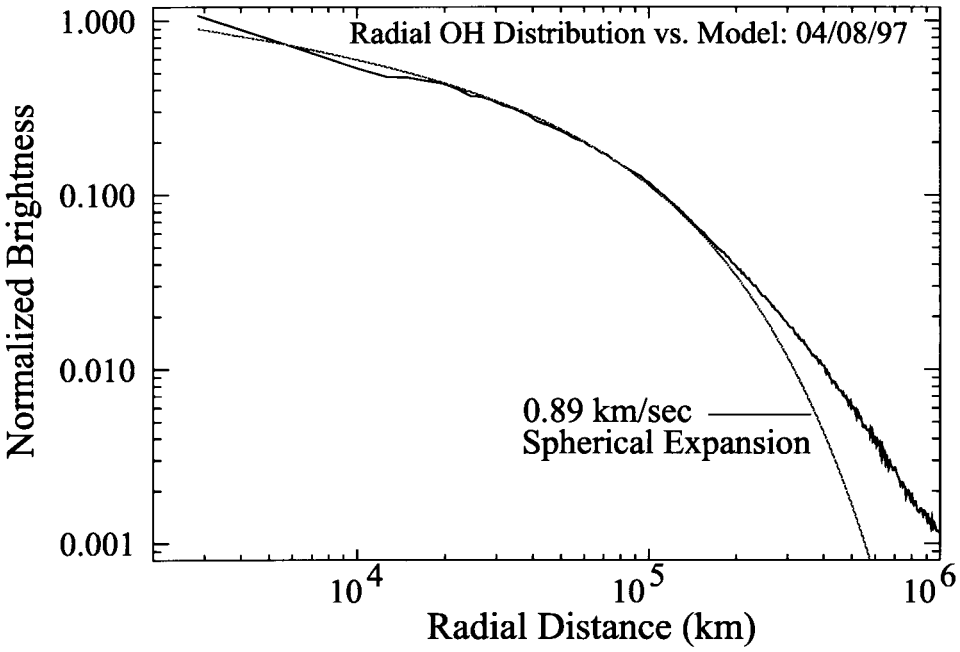

Figure 1. The azimuthally averaged radial distribution of ground state NUV OH emission from comet Hale–Bopp is compared with a two-component spherical expansion simulation for a typical outflow velocity of 1 km/s. Note the failure of the model to produce the observed emission in the outer coma.

reactions (Komitov, 1989) and excitation from collisions with neutral and charged particles inside the sphere (e.g., Bhardwaj, 1999).

5. Observational Evidence for Collisions in Hale–Bopp

Evidence for strong collisional effects in the coma of Hale–Bopp is pervasive in the data that has been presented to date. Clear signatures of this are found in the radial distribution of neutral emissions, the brightness of diagnostic metastable emission lines, the measured acceleration of ions, and in the emission line widths of key diagnostic species. In particular:

Radial Distributions. The radial extent of the coma in all primary species is consistent with a significantly higher outflow velocity than previous comets. In particular, OH cannot be fit with a 1 km/s outflow (Figure 1), but requires V_{OH} between 2.5 and 3.5 km/s to reach the radial distances where it is observed (Harris et al., 2002). Similar wide field measurements of C (λ1657) (Harris et al., 1999) and metastable O(^{1}D) (Morgenthaler et al., 2001) show comparable radial extensions consistent with substantial acceleration in the coma.

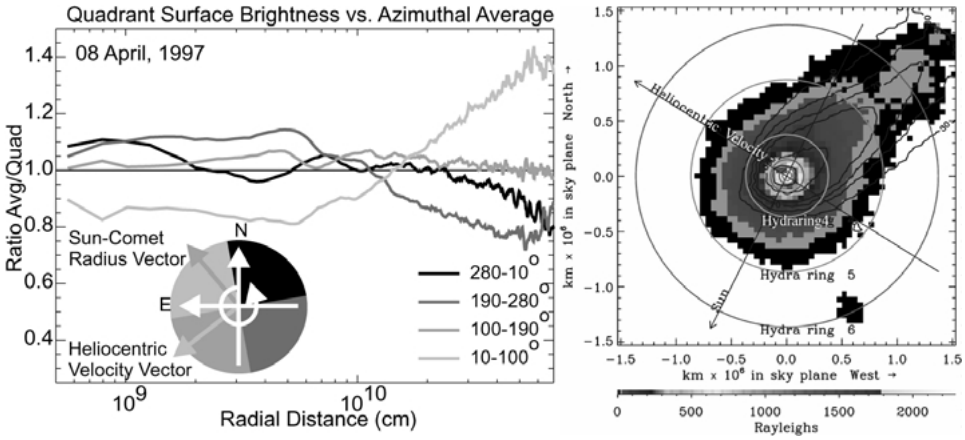

Figure 2. A continuum subtracted image of O(^{1}D) emission from Hale–Bopp and normalized radial quadrant ring summation of the OH distribution both show evidence of extended emissions in a region between the orbit trailing and anti-sunward directions. In neither case can the emission be tied to a secondary gas production source or dust contamination, but instead appear to be the result of a vectored acceleration in this area of the coma.

Metastable Emissions. Because the de-excitation of atoms and molecules in metastable states occurs very close to the location where they are formed, they effectively trace location of photochemistry in the coma. The radial distribution of metastable O(^{1}D), which is produced primarily from H_2O and OH dissociation was measured in Hale–Bopp. In addition, C(^{1}D), which is produced from CO dissociation was observed with a course aperture summation technique at points on and off the nucleus (Oliversen et al., 2002). Both species support the presence of a substantial collisional coma. The inner coma spatial distribution of O(^{1}D) can only be fit by models that include substantial quenching of the emission inside the collision sphere (Morgenthaler et al., 2001), while the C(^{1}D) emission was sharply *peaked* on the nucleus despite a substantially far longer metastable lifetime (4077 s) than O(^{1}D) (150 s). The aperture summation technique used for C(^{1}D) contains no radial information inside the aperture, and so it was not possible to determine how the C(^{1}D) emission was distributed in the inner coma. However, Oliversen et al. (2002) note that several collisional mechanisms could stimulate the emission at rate equal to or faster than quenching (Bardhwaj, 1999), an idea first proposed for C (λ1931) emission from comet West (Feldman, 1978).

Ion Acceleration. Observations of H_2O^+ velocity gradients in the inner coma suggest acceleration less than half that measured from Halley and other comets (Anderson, 1999). Anderson (1999) suggests that mass loading of solar wind by comet ions could account for the retardation, however, Harris et al. (2002) note that ion-neutral interactions in the collision sphere might produce a similar effect, and

could account for an asymmetry seen in the anti-sunward coma radial distributions of OH and O(^{1}D) (Figure 2).

Velocity Profiles. Velocity resolved observations of radio emission lines were obtained from several species in the coma of Hale–Bopp, including OH, HCN, Hα, and others (Biver et al., 1999; Colom et al., 1999). All of these show signatures of acceleration. Coma averaged measurements of the average HCN emission line width inside 10^4 km (Biver et al., 1999) translate to velocities (V = 1.4 km/s) that are >50% greater than weaker comets, while the outer coma measurements of ($R > 5 \times 10^5$ km) OH (Colom et al., 1999; Schloerb et al., 1999) give velocities (V = 2.2 km/s) that are nearly twice as large. These results are both consistent with the presence of acceleration over much of the coma. High spectral resolution measurements of the Hα emission line from Hale–Bopp, which has components with excess velocities of 8 km/s from OH dissociation (Keller, 1976) and 25 km/s from H_2O (Combi et al., 2000), show a line shape that is narrower than expected based on the known rates of H_2O and OH photochemistry (Morgenthaler et al., 2002b). Such a narrowing is also consistent with thermalization of very fast H atoms with slower neutrals in the collisional coma.

6. Wide Field Observations

Wide field observations offer a means to determine the gas production rate and velocity structure from the coma brightness distribution and modified versions of spherical expansion models. The principal advantage of a very wide field is that the entire coma is included in the observation. This removes ambiguity about the total fraction of the emission being beyond the sampled region, the amount of which depends on the unknown outflow velocity. When the entire coma is sampled, then simple field summed photometry can be inverted directly to production via:

$$Q_x = \frac{10^6 I_x \Omega \Delta^2}{\tau_x g_x}, \tag{2}$$

where Ω is the solid angle of the FOV, Δ is the geocentric distance, τ_x is the lifetime of species x, and I_x is the brighness across the field of view, and g_x is emission line fluorescence efficiency. For metastable O(^{1}D) emission, which emits only once, Equation (2) becomes

$$Q_{\mathrm{O}(^1\mathrm{D})} = \frac{4}{3} 4\pi \Omega \Delta^2 I_{\lambda 6300} \tag{3}$$

(Schultz et al., 1993). In each case the production rate depends on factors unrelated to the velocity structure and spatial distribution of the coma.

Examples (Table I) of wide-field aperture summation production rate inversion in Hale–Bopp include C (λ1657) imaging (Harris et al., 1997), O(^{1}D) imaging

TABLE I

Hale–Bopp gas production rates from wide field aperture summation

Species	Date	Q_x^{30} ($\times 10^{30}$ s^{-1})
OH(NUV)[a]	04/08/97	$Q_{\rm OH}^{30}$ 9.3 ($\pm$ 1.4)
OH(radio)[b]	04/02–08/97	$Q_{\rm OH}^{30}$ 9.4 ($\pm$ 1.5)
C(λ1657)[c]	04/08/97	$Q_{\rm C}^{30}$ 2.6 ($\pm$ 1.2)
H(λ1215)[d]	04/07/97	$Q_{\rm H}^{30}$ 9.5 ($\pm$ 0.9)

[a] Harris et al., 2002.
[b] Colom et al., 1999.
[c] Harris et al., 1997.
[d] Combi et al., 2000.
Adapted from their published $Q_{\rm H_2O}$.

and integral field spectroscopy (Morgenthaler et al., 2001), H Ly-α with SOHO (Combi et al., 2000), and OH in the NUV (Harris et al., 2002) and radio (corrected for quenching) (Colom et al., 1999). The $Q_{\rm O(^1D)}$ can be used to determine the H_2O production rate by adding a term to the equation that includes the branching ratios (B_{H_2O} and B_{OH}) from its parents. Except for radio OH measurements, these observations were all 2-dimensional images with velocity information in the radial extent of the emission. Once the production rate is determined from the full coma inversion, it serves as a boundary condition for using expansion models to determine the outflow velocity.

Modeling the Velocity Distribution. When the imaging data contains a full radial brightness distribution, the velocity structure can be constrained using modified versions of simple, spherical expansion models that account for collisional acceleration. The outer portion of the profile shape, which depends most strongly on the outflow velocity, combines with the boundary imposed by the production rate determination using the summation method to converge the results of model simulations toward a single result. In the wide field images obtained as part of the University of Wisconsin–Goddard Space Flight Center Hale–Bopp observing campaign (Morgenthaler et al., 2002a), Harris et al. (2002) used two variations of the two-component Haser model to determine the amount and extent of the acceleration, along with the velocities at the boundaries of the OH and O(^{1}D) radial profiles (Harris et al., 2002; Morgenthaler et al., 2001).

In one approach the radial profiles may be treated using a classic two-component Haser model (Krishna Swamy, 1997), where the acceleration is treated as a difference between fixed OH and H_2O velocities. The results of this model will converge tightly to a small range of values shown in Figure 3, however they imply a greater production rate ($Q_{\rm H_2O\text{-}model} = 1.4 \times 10^{31}$ s^{-1} vs. $Q_{\rm H_2O\text{-}aperture} = 1.1$

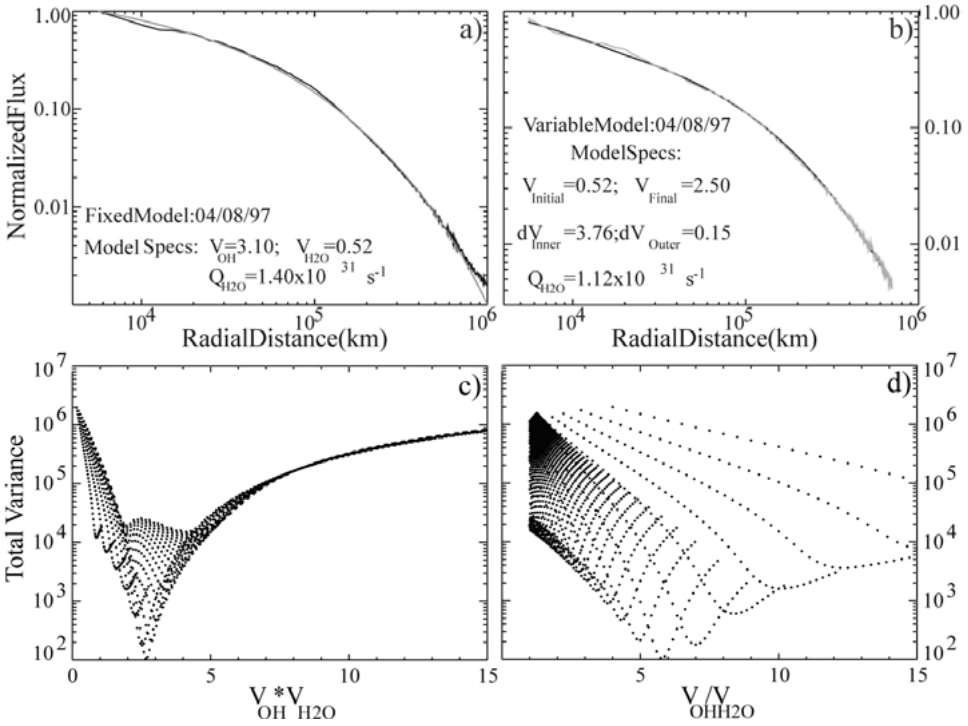

Figure 3. The fit to the observed radial distribution of OH for each model is shown in a and b, while c and d show a graphical representation of the convergence to a small range of values in the fixed case. Both models fit the profile, the accelerating model produces velocities and production rate values more consistent with direct measurements of these quantities (Table II). Below the profile matches the quality of the point-by-point variance of the comparison between various model runs and the data are shown as a function of the velocity product c) and ratio d). Note the sharp convergence to a velocity product of 2.5 that indicates acceleration from the inner to outer coma.

$\times\ 10^{31}\ \mathrm{s}^{-1}$) and both a smaller initial velocity (0.5 km/s vs. 1.4 km/s) and higher final velocity (3.35 km/s vs. 2.2 km/s) than were observed in the radio (Biver et al., 1999; Colom et al., 1999).

An improvement over the fixed velocity model results is obtained if the 2 component equations are modified to permit linear accelerations with different gradients inside and outside the region where collisions fully dominate, all while keeping $V_{\mathrm{OH}} = V_{\mathrm{H_2O}}$. The addition of the collision sphere diameter as a third parameter reduces the convergence of the results compared to the fixed case. However, the quality of the fit is better overall and both the production rates and velocities are more consistent with other estimates (Table II, Figure 3). Confidence in the veracity of this method is bolstered by the fact that the closest match to the radial profile also inverts to the observed production rate, and by the fact that models reproduce the aperture averaged velocities obtained in radio measurements (Colom et al., 1999; Biver et al., 1999).

TABLE II

Characteristics of water production in an accelerating coma from spherical expansion models are compared with summation measurements of brightness and velocity. The model results in the inner and outer coma are isolated to regions comparable to those sampled in radio observations

Source	$V_{\text{Inner Coma}}$	$V_{\text{Outer Coma}}$	$Q^{31}_{H_2O}$ ($\times 10^{31}$ s^{-1})
OH summation[a]	–	–	1.1 ($\pm$ 0.16)
OH radio[b]	–	2.2 km/s	–
HCN radio[c]	1.2 km/s	–	–
Fixed model[a,d]	0.5 km/s	3.5 km/s	1.4
Accel. model[a]	1.4 km/s	2.3 km/s	0.93

[a] Harris et al., 2002.
[b] Colom et al., 1999.
[c] Biver et al., 1999.
[d] Morgenthaler et al., 2001.

7. Summary and Conclusions

By virtue of its very high gas production rate, comet Hale–Bopp provided a unique opportunity to observe the effects of collisional heating on the velocity, thermal, and chemical characteristics of the coma. While these effects are easily identifiable in this case, the important points to be taken are that the collision sphere should be accounted for in *any* active comet and that the manner in which the collision sphere affects the coma depends on a synergy of processes (e.g., gas production rate, gas species photochemical lifetime, opacity to solar UV radiation, heliocentric velocity and distance). As a result each comet must be evaluated on the basis of its individual circumstances at the time observation, a significant departure from the one-size-fits-all approach that works for less active bodies. There is limited observational evidence from a steady increase of the coma averaged outflow velocity (Bockelée-Morvan et al., 1990; Cochran and Schleicher, 1993) that the point where collisions begin to take hold is for $Q_{H_2O} \gtrsim 10^{29}$ s^{-1}. From that turn up point to the Hale–Bopp production rate, the size of the sphere will expand until it encompasses the entire water scale length, at which point the coma will be largely thermalized. In between, the observed velocity will be a mix of a thermalized component and the vectorialized ballistic flow seen in weak objects. For extreme (as yet unobserved) cases with $Q_{H_2O} \gtrsim 10^{31}$ s^{-1}, opacity effects may prevent significant photochemistry in the deep collision sphere, which may actually reduce the effect compared to Hale–Bopp.

Acknowledgements

The authors wish to acknowledge the efforts of many observers who participated in UW-GSFC observing program that produced the data set that forms the basis of this work. These team members include E. Mierkiewicz, M. Vincent, C. Woodward, N. Doane, and F. Roesler. This research was supported under NASA grant NAGW-7952 to the University of Wisconsin-Madison.

References

Anderson, C. M.: 1999, *Earth Moon Planets* **78**, 99–104.
Bhardwaj, A. 1999, *J. Geophys. Res.* **104**, 1929–1942.
Biver, N., et al.: 1999, *Earth Moon Planets* **78**, 5–11.
Bockelée-Morvan, D., Crovisier, J., and Gerard, E. 1990, *Astron. Astrophys.* **238**, 382–400.
Budzien, S. A., Festou, M. C., and Feldman, P. D.: 1994, *Icarus* **107**, 164–188.
Cochran, A. L. and Schleicher, D. G.: 1993, *Icarus* **105**, 235–253.
Colom, P., Gerard, E., Crovisier, J., Bockelée-Morvan, D., Biver, N., and Rauer, H.: 1999, *Earth Moon Planets* **78**, 37–43.
Combi, M. R., Bos, B. J., and Smyth, W. H.: 1993, *Ap. J.* **408**, 668–677.
Combi, M. R., Kabin, K., DeZeeuw, D. L., Gombosi, T. I., and Powell, K. G.: 1999, *Earth Moon Planets* **79**, 275–306.
Combi, M. R., Reinard, A. A., Bertaux, J.-L., Quemerais, E., and Mäkinen, T.: 2000, *Icarus* **144**, 191–202.
Craven, J. D. and Frank, L. A.: 1987, *Astron. Astrophys.* **187**, 351–356.
Dello Russo, N., Mumma, M. J., DiSanti, M. A., Magee-Sauer, K., Novak, R., and Rettig, T. W.: 2000, *Icarus* **143**, 324–337.
Feldman, P. D.: 1978, *Astron. Astrophys.* **70**, 547–553.
Feldman, P. D. and Brune, W. H.: 1976, *Ap. J.* **209**, L45–L48.
Feldman, P. D. et al.: 1987, *Astron. Astrophys.* **187**, 325–332.
Festou, M. C.: 1981, *Astron. Astrophys.* **95**, 69–79.
Harris, W. M., Nordsieck, K. H., Scherb, F., and Mierkiewicz, E. J.: 1999, *Earth Moon Planets* **78**, 161–167.
Harris, W. M., Scherb, F., Mierkiewicz, E. J., Oliversen, R. J., and Morgenthaler, J. P.: 2002, *Ap. J.* **578**, 996.
Haser, L.: 1957, *Bull. Soc. Roy. Sci. Liege* **43**, 740–750.
Hodges, R. R.: 1990, *Icarus* **83**, 410–433.
Huebner, W. F., Keady, J. J., and Lyon, S. P.: 1992, *Astrophys. Space Sci.* **195**, 7–125.
Keller, H.: 1976, *Space Sci. Rev.* **18**, 641–684.
Komitov, B.: 1989, *Adv. Space Res.* **9**, 177–179.
Krishna Swamy, K. S.: 1997, *Physics of Comets*, World Scientific, Singapore, 310 pp.
McFadden, L. A., A'Hearn, M. F. Edsall, D. M., Feldman, P. D., Roettger, E. E., and Butterworth, P. S.: 1987, *Astron. Astrophys.* **187**, 333–338.
Morgenthaler, J. P., Harris, W. M., Scherb, F., Anderson, C. M., Oliversen, R. J., Doane, N. E., Combi, M. R., Marconi, M. L., and Smyth, W. H.: 2001, *Ap. J.* **563**, 451–461.
Morgenthaler, J. P., Harris, W. M., Roesler, F. L., Scherb, F., Anderson, C. M., Doane, N. E., and Oliversen, R. J.: 2002a, these proceedings.
Morgenthaler, J. P., Harris, W. M., Scherb, F., Doane, N. E., and Oliversen, R. J.: 2002b, these proceedings.

Oliversen, R. J., Doane, N. E., Scherb, F., Harris, W. M., and Morgenthaler, J. P.: 2002a, *Ap. J.* **581**, in press.
Schleicher, D. G. and A'Hearn, M. F.: 1988, *Ap. J.* **331**, 1058–1077.
Schloerb, F. P.: 1988, *Ap. J.* **332**, 524–530.
Schloerb, F. P., Devries, C. H., Lovell, A. J., Irvine, W. M., Senay, M., and Wootten, H. A.: 1999, *Earth Moon Planets* **78**, 45–51.
Schultz, D., Li, G. S. H., Scherb, F., and Roesler, F. L.: 1993, *Icarus* **101**, 95–107.
Whipple, F. L. and Huebner, W. F.: 1976, *Annu. Rev. Astron. Astrophys.* **14**, 143–172.